J. Bowman, C. M. Yentsch, W. T. Peterson, Eds. (Springer-Verlag, Berlin, 1986), pp. 193–223.
19. The processes responsible for the shape of the curves in Fig. 2 are not known.
20. P. F. Sale, *Environ. Biol. Fish.* **3**, 85 (1978); P. K. Dayton, in *Ecological Processes in Coastal and Marine Systems*, R. J. Livingston, Ed. (Plenum Press, New York, 1979), pp. 3–18; M. A. Kendall, R. S. Bowman, P. Williamson, J. R. Lewis, *Neth. J. Sea Res.* **16**, 119 (1982); A. J. Underwood and E. J. Denley, in *Ecological Communities: Conceptual Issues and the Evidence*, D. R. Strong, Jr., D. Simberloff, L. G. Abele, A. B. Thistle, Eds. (Princeton Univ. Press, Princeton, NJ, 1984), pp. 151–180; J. Roughgarden, S. Gaines, H. Possingham, *Science* **241**, 1460 (1988).
21. P. M. Yoshioka, *Ecology* **63**, 457 (1982).
22. Because of the obviously nonnormal distribution of the data a nonparametric test was used. Each daily settlement value consisted of the average of two or three settlement plates per site. One site was observed from 29 April until 8 August 1989; the Spearman correlation coefficients between settlement and water temperature anomaly were −0.258 for *Chthamalus* and −0.223 for *Pollicipes* (overall), whereas those from 1 June to 29 August were −0.266 and −0.400. Coefficients from the other site, observed from 3 June until 27 July, were −0.274 for *Chthamalus* and −0.482 for *Pollicipes*. All correlation coefficients are significantly different from 0 at $\alpha = 0.025$ (one tail). Small magnitude of correlation values might reflect uncertainty of the offshore larval reservoir, differential behavior of internal bores at the Scripps Pier and Dyke Rock, unrecorded large-event bores, or other phenomena affecting settlement.
23. L. R. Haury, M. G. Briscoe, M. H. Orr, *Nature* **278**, 312 (1979).
24. A. M. Barnett and A. E. Jahn, *Cont. Shelf Res.* **7**, 1 (1987).
25. P. E. Smith and R. W. Eppley, *Limnol. Oceanogr.* **27**, 1 (1982).
26. J. Pineda, unpublished observations.
27. I thank P. Dayton, J. Enright, L. Haury, M. Tegner, E. Vetter, and C. Winant, and two reviewers for constructive comments on the manuscript. I also thank many divers who helped sample. Temperature data were supplied by the Scripps Institution of Oceanography. E. del Castillo supported me in every stage of the research. I especially wish to thank the people of Mexico who supported this research through a CONACYT graduate fellowship which also covered research expenses. I also acknowledge grants from NSF to P. K. Dayton and from MMS to C. D. Winant.

4 February 1991; accepted 16 May 1991

A Component of Calcium-Activated Potassium Channels Encoded by the *Drosophila slo* Locus

NIGEL S. ATKINSON,* GAIL A. ROBERTSON, BARRY GANETZKY

Calcium-activated potassium channels mediate many biologically important functions in electrically excitable cells. Despite recent progress in the molecular analysis of voltage-activated K^+ channels, Ca^{2+}-activated K^+ channels have not been similarly characterized. The *Drosophila slowpoke* (*slo*) locus, mutations of which specifically abolish a Ca^{2+}-activated K^+ current in muscles and neurons, provides an opportunity for molecular characterization of these channels. Genomic and complementary DNA clones from the *slo* locus were isolated and sequenced. The polypeptide predicted by *slo* is similar to voltage-activated K^+ channel polypeptides in discrete domains known to be essential for function. Thus, these results indicate that *slo* encodes a structural component of Ca^{2+}-activated K^+ channels.

POTASSIUM CHANNELS COMPRISE A large and diverse group of integral membrane proteins that determine the level of excitability and the repolarization properties of neurons and muscle fibers (*1*). On the basis of gating mechanisms K^+ channels can be subdivided into at least two distinct classes: voltage-activated K^+ channels respond to changes in membrane potential, whereas the gating of Ca^{2+}-activated K^+ channels is dependent on intracellular Ca^{2+}, although members of this class are also sensitive to voltage. Ca^{2+}-activated K^+ channels occur in neurons, muscles, and secretory cells of vertebrates and invertebrates and govern action potential repolarization, the rate and pattern of repetitive firing, and Ca^{2+} entry (*2*).

Laboratory of Genetics, University of Wisconsin, Madison, WI 53706.

*Present address: Department of Zoology, University of Texas, Austin, TX 78712.

The molecular analysis of K^+ channels was initiated by the cloning of the *Drosophila Shaker* (*Sh*) locus, a gene encoding one class of voltage-activated K^+ channels (*3*). Subsequently, many K^+ channel genes were cloned from various organisms on the basis of sequence similarity with *Sh*, enabling elucidation of important structural features essential to K^+ channel activity (*4*). However, none of these genes appears to encode a K^+ channel gated by Ca^{2+}

In *Drosophila*, a fast, Ca^{2+}-activated K^+ current, I_{CF}, has been identified in adult and larval muscles and in larval neurons (*5–7*). Like the BK class of Ca^{2+}-activated K^+ channels in mammalian muscle (*8*), the *Drosophila* channels that conduct I_{CF} are sensitive to charybdotoxin and have a relatively large single channel conductance (*6, 7*). Mutations of the *slo* locus specifically eliminate I_{CF} (*6, 7, 9*). To determine if *slo* encodes a structural component of Ca^{2+}-activated K^+ channels or perhaps affects their function by some other means, we undertook a molecular analysis of this locus (*10*).

We first pinpointed the cytological location of the gene, defined on the basis of a single, cytologically normal mutation, slo^1 (*6*). We mapped this mutation by meiotic recombination to position 90.0 on the third chromosome between *bar-3* (map position 79.1) and *taxi* (map position 91), corresponding to polytene chromosome region 95-96 (*11*). To refine this location, we isolated three γ-ray induced *slo* mutations (slo^3, slo^4, and slo^8) on the basis of their failure to complement the slo^1 behavioral phenotype (*6, 12*) (Table 1). The *slo* phenotype of these new mutations was confirmed electrophysiologically (*13*).

Cytological examination of these mutations revealed that all contained chromosome rearrangements with a common breakpoint at polytene band 96A17 (Table 1). These results together with the cytological and genetic characterization of other chromosome lesions in this region, originally isolated by other criteria, identify band 96A17 as the cytological location of *slo* (Table 1).

One of the breakpoints in the slo^4 inversion is at the *slo* locus and the other is at 96F5-8 close to the previously cloned *E(spl)* locus (*14*). We were thus able to use this inversion to clone genomic DNA from the *slo* locus by chromosome walking and jumping (*15*). Chromosomal in situ hybridization of two sets of phage clones from existing chromosome walks in the *E(spl)* region revealed that one set was proximal and the other set distal to the 96F5-8 breakpoint. Consequently, we extended the proximal walk by isolating overlapping cosmids from a wild-type library until the 96F5-8 breakpoint was reached. To identify a cosmid spanning the inversion breakpoint (Fig. 1A), we assayed each cosmid from the walk

Table 1. Summary of chromosome aberrations used in cytological mapping of the *slo* locus.

Name	Cytological lesion	*slo* phenotype
slo^1	Normal	Mutant
slo^3	Deletion (95E6-7 to 96A18)	Mutant
slo^4	Inversion (96A17 and 96F5-8)	Mutant
slo^8	Deletion (96A2-9 to 96D2-4)	Mutant
Df(3R)S87-5	Deletion (95F7-9 to 96A17-18)	Mutant
Df(3R)S87-4	Deletion (95E8-F1 to 95F15-96A2)	Normal
T(Y;3)A117	Translocation (broken at 96A10-17)	Mutant

by chromosomal in situ hybridization to *slo*^{4} homozygotes: a cosmid spanning the breakpoint should hybridize to both ends of the inversion, whereas cosmids that stop short of this break should hybridize to a single site. DNA disrupted by the inversion was further delimited by in situ hybridization and Southern blot analysis to a 3-kb Eco RI restriction fragment within this cosmid. In *slo*^{4}, the 3-kb Eco RI genomic fragment at 96F5-8 is broken into two parts, each juxtaposed to DNA sequences from the *slo* locus at 96A17. A phage containing one of these junction fragments was isolated by probing a *slo*^{4} genomic library with the 3-kb wild-type Eco RI fragment. This junction fragment was subsequently used to initiate a chromosome walk in a wild-type cosmid library to obtain genomic DNA that included the *slo* locus (Fig. 1B).

An approximate location of the *slo* transcription unit was defined by the 96A breakpoint of *slo*^{4}, which mapped to a 3-kb Eco RI–Hind III genomic fragment. We used this fragment to screen cDNA libraries from *Drosophila* heads. One cDNA, Z8, hybridized to both sides of the *slo*^{4} inversion and also to both parts of the *T(Y;3)A117* translocation (Fig. 2, A and B). The fact that Z8 spans two different *slo* mutations demonstrates that this cDNA is derived from the *slo* transcript. Two transcripts of 5.8 kb and 11 kb are detected by Z8 probes on Northern blots of polyadenylated [poly(A)$^+$] RNA isolated from heads (Fig. 2C). The absence of these transcripts in *slo*^{4} homozygotes (Fig. 2C) identifies them as *slo* transcripts. We do not know whether the two wild-type transcripts encode different *slo* polypeptides.

Because Z8 is incomplete (see below), we

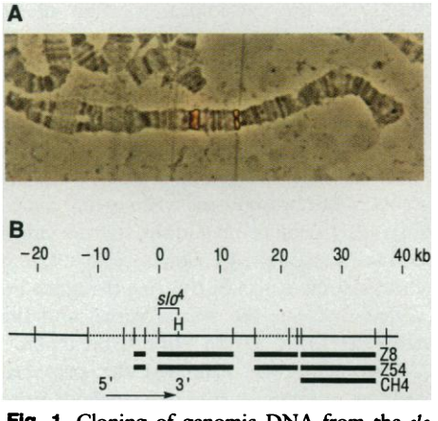

Fig. 1. Cloning of genomic DNA from the *slo* locus. (**A**) Hybridization of a cosmid from the genomic walk to polytene chromosomes of *slo*^{4} homozygotes (*34*). (**B**) An Eco RI map of the cloned region. The position of the *slo*^{4} inversion breakpoint is indicated. H, the Hind III site that marks the rightward limit of the restriction fragment containing the breakpoint; black bars, the genomic restriction fragments that hybridize with *slo* cDNAs Z54, Z8, and CH4 (see text and Fig. 3). (The presence of a black bar indicates only that the corresponding restriction fragment above the bar contains one or more exons of unknown size. Because the cDNAs lack internal Eco RI sites, a break between bars indicates the presence of an intron in genomic DNA that is spliced out in the cDNAs.) Broken lines, regions where the order of the restriction fragments has not been determined so the distance between exons is not known. The entire *slo* locus must extend beyond the limits shown because the cDNAs hybridize to genomic restriction fragments not contained in the cloned region and because the *T(Y;3)A117* breakpoint lies outside the limits of the chromosome walk. The direction of transcription relative to the chromosome walk was determined from Northern blots by using single-stranded RNA probes.

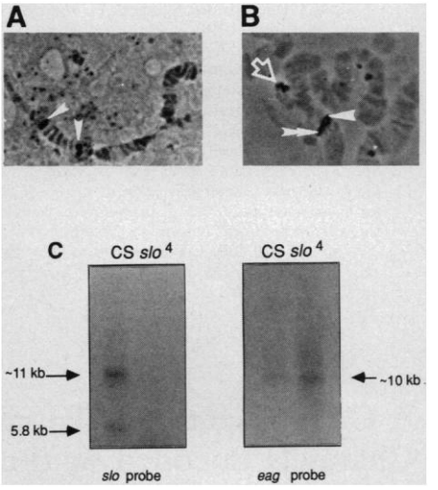

Fig. 2. Identification of the *slo* transcription unit. (**A**) Hybridization of cDNA Z8 to polytene chromosomes homozygous for the *slo*^{4} inversion. Arrowheads, hybridization signals at inversion end points. (**B**) Hybridization of cDNA Z8 to polytene chromosomes heterozygous for the *T(Y;3)A117* translocation and a normal third chromosome. A hybridization signal (arrowhead) is seen at the intact *slo* locus on the normal chromosome. In addition, both the proximal (double arrowhead) and distal parts (open arrow) of the translocated chromosome contain sites that hybridize. In this preparation part of the distal piece of the translocation has asynapsed from the normal chromosome. (**C**) Northern blot analysis of *slo* transcripts. Approximately 10 μg each of poly(A)$^+$ RNA isolated from heads of Canton S (CS) and homozygous *slo*^{4} adults was loaded into individual lanes. The filter was probed with ^{32}P-labeled cDNA Z8 (left). Similar results were obtained when blots were probed with either purified fragments of Z8 lacking any intron sequences or single-stranded RNA transcribed from the T7 promoter of the pBluescript SK$^-$ (Stratagene) plasmid that carried cDNA Z8. Single-stranded probes transcribed in the reverse orientation from the SP6 promoter of Z8 did not detect any transcripts (not shown). As a control, the blot was stripped and reprobed with an *eag* cDNA (right). Experimental conditions were as described (*26*).

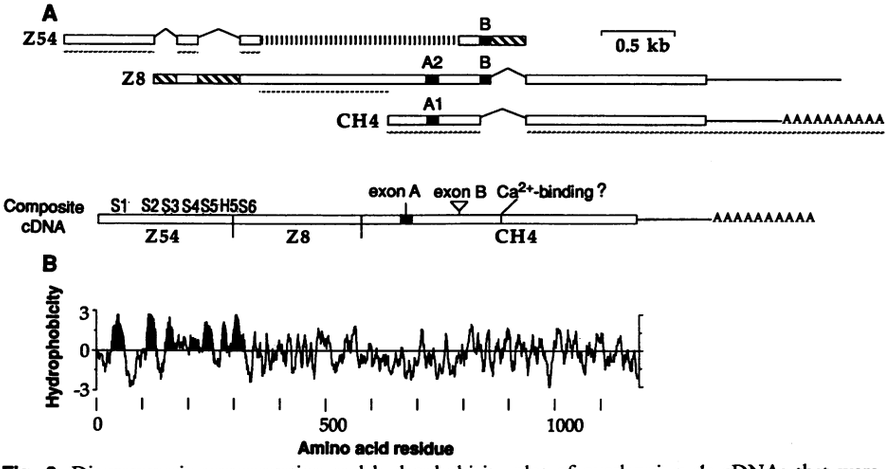

Fig. 3. Diagrammatic representation and hydrophobicity plot of overlapping *slo* cDNAs that were assembled to yield a composite sequence. (**A**) The three cDNAs drawn to scale. Dashed underlines, cDNA segments that were assembled into the composite shown below; open boxes, open reading frames; hatched boxes, introns that were not spliced out of some cDNAs (*17*). The open reading frame of Z54 is preceded by an untranslated segment (not shown) that may also represent an unspliced intron (*17*). All the regions shown have been completely sequenced on both strands (*16*), with the exception of the central segment of Z54 (interrupted bar), which has not been sequenced. For those regions that have been fully sequenced, the nucleotide sequences in overlapping segments are identical except for the unspliced introns and the two sites of alternative splicing indicated. At site A an exon encoding 14 amino acids (A1) that is present in CH4 is replaced by a different exon encoding 25 amino acids (A2) in Z8. At site B an exon 22 amino acids long is present in Z54 and Z8 but lacking in CH4. Z8, which does not end in a poly(A)$^+$ tail, extends beyond the poly(A)$^+$ tail present in CH4 suggesting the presence of alternative polyadenylation sites. (**B**) Hydropathy plot for the deduced *slo* polypeptide (Fig. 4) encoded by the composite cDNA. The plot has been aligned with the composite cDNA sequence above. Hydrophobicity values were calculated according to Kyte and Doolittle (*19*) with a window size of nine amino acids. The seven shaded hydrophobic peaks were named according to the corresponding domains of other K$^+$ channels after aligning sequences of the fourth and sixth hydrophobic peaks with S4 and H5, respectively.

used it as a probe to isolate the overlapping cDNAs, Z54 and CH4. Although none of these cDNAs contains a complete open reading frame (ORF), together they yield a composite sequence capable of specifying a polypeptide over 1100 amino acids in length (Fig. 3A). These cDNAs represent a spliced transcript encompassing over 40 kb of genomic DNA as indicated by Southern analysis (Fig. 1B).

The nucleotide sequence of the composite *slo* cDNA (Fig. 3) is 4232 nucleotides (*16*) with an open reading frame (between positions 1 and 3552) that encodes a deduced polypeptide at 1184 amino acids (Fig. 4). This sequence appears incomplete at the 5′ end (*17*) but complete at the 3′ end because the untranslated tail of CH4 terminates in a run of adenine residues preceded by the polyadenylation signal AATAA (*18*).

Hydropathy analysis (*19*) revealed seven hydrophobic domains near the NH_2-terminus of the *slo* polypeptide (Slo) similar to the structure of other known K^+ channel polypeptides (*4*). The fourth hydrophobic segment of Slo is similar to the S4 domain in voltage-gated channels, which is thought to mediate voltage sensitivity. The S4 motif is characterized by a positively charged residue at every third position separated by two hydrophobic residues (*20*). Out of 26 positions in the alignment of S4 domains from Slo and Shaker, there are six amino acid identities and four conservative substitutions. This region of Slo shows a slightly better alignment with an S4 domain of rat brain Na^+ channels, yielding seven identities and four conservative substitutions (Fig. 5A). The Slo S4 domain contains fewer positive charges than S4 domains in voltage-gated channels but the functional significance of this is not known. The presence of an S4 domain in a guanosine 3′,5′-monophosphate (cGMP)–gated channel has led to the suggestion that the S4 sequence contributes to the basic architecture of various channels in addition to its function as a voltage sensor (*21*).

The greatest similarity between Slo and K^+ channel polypeptides is in the H5 domain, an integral part of the ion conduction pore (*22–25*). When aligned with an H5 consensus sequence for the *Sh* superfamily, Slo shares 11 identities and five conservative substitutions out of 25 positions (Fig. 5B). This alignment is centered on a core of 11 amino acids in which there are nine identities and two conservative substitutions. Moreover, at five positions in the H5 domain where Slo deviates from the consensus, it shares identities with Eag, another *Drosophila* K^+ channel polypeptide identified by means of genetic strategies (*26, 27*). These relations indicate that *slo* and other K^+ channel genes have evolved from a common ancestor.

One of the conservative changes within the H5 domain of Slo with respect to the *Sh* family consensus is a substitution of serine for threonine at position 284. Creation of the same replacement in *Sh* by site-directed mutagenesis results in a tenfold decrease in sensitivity to internal tetraethylammonium (TEA) blockade (*23*). This result is consistent with the observation that, in vivo, I_{CF} is relatively insensitive to internal TEA ($K_d \approx 100$ mM) (*28*). Site-directed mutations in *Sh* that alter ionic selectivity and increase sensitivity to external TEA also occur naturally at the equivalent positions in the *slo* sequence (*24, 25*). For example, the presence of tyrosine at position 292 would be predicted to result in a high sensitivity of I_{CF} to external TEA blockade (*25*). These properties have not yet been empirically

```
   1  GMSGCDQSTV ESLADDPTDS PFDADDCLKV RKYWCFLLSS IFTFLAGLLV
                                        ──── S1 ────
  51  VLLWRAFAFV CCRKEPDLGP NDPKQKEQKA SRNKQEFEGT FMTEAKDWAG
 101  ELISGQTTTG RILVVLVFIL SIASLIIYFV DASSEEVERC QKWSNNITQQ
                  └──── S2 ────┘
 151  IDLAFNIFFM VYFFIRFIAA SDKLWFMLEM YSFVDYFTIP PSFVSIYLDR
      └──────── S3 ────────┘                              └──
 201  TWIGLRFLRA LRLMTVPDIL QYLNVLKTSS SIRLAQLVSI FISVWLTAAG
      ──────── S4 ────────┘          #  └──── S5 ────
 251  IIHLLENSGD PLDFDNAHRL SYWTCVYFLI VTMSTVGYGD VYCETVLGRT
      ──┘                            └──────── H5 ────────┘└
 301  FLVFFLLVGL AMFASSIPEI IELVGSGNKY GGELKREHGK RHIVVCGHIT
      ──────── S6 ────────┘
 351  YESVSHFLKD FLHEDREDVD VEVVFLHRKP PDLELEGLFK RHFTTVEFFQ
 401  GTIMNFIDLQ RVKVHEADAC LVLANKYCQD PDAEDAANIM RVISIKNYSD
                                                  #
 451  DIRVIIQLMQ YHNKAYLLNI PSWDWKQGDD VICLAELKLG FIAQSCLAPG
 501  FSTMMANLFA MRSFKTSPDM QSWTNDYLRG TGMEMYTETL SPTFIGIPFA
                  #
 551  QATELCFSKL KLLLLAIEIK GAEEGADSKI SINPRGAKIQ ANTQGFFIAQ
 601  SADEVKRAWF YCKACHEDIK DETLIKKCKC KNLTVQPRSK FDDLDEHHPA
                                        └ Alt. Exon A1 ┘
 651  PTFTPPELPK RVHVRGSVSG DITRDREDTN LLNRNVRRPN GTGNGTGGMH
                                                  • • •
 701  HMNNTAAAAA AAAAAGKQVN KVKPTVNVSR QVEGQVISPS QYNRPTSRSS
                      •                 Alt. Exon B ┘  #
 751  GTGTQNQNGG VSLPAGIADD QSKDFDFEKT EMKYDSTGMF HWSPAKSLED
                      *  *  *  *  *
 801  CILDRNQAAM TVLNGHVVVC LFADPDSPLI GLRNLVMPLR ASNFHYHELK
 851  HVVIVGSVDY IRREWKMLQN LPKISVLNGS PLSRADLRAV NVNLCDMCCI
 901  LSAKVPSNDD PTLADKEAIL ASLNIKAMTF DDTIGVLSQR GPEFDNLSAT
       #                                    #
 951  AGSPIVLQRR GSVYGANVPM ITELVNDGNV QFLDQDDDDD PDTELYLTQP
                  ■
1001  FACGTAFAVS VLDSLMSTTY FNQNALTLIR SLITGGATPE LELILAEGAG
1051  LRGGYSTVES LSNRDRCRVG QISLYDGPLA QFGECGKYGD LFVAALKSYG
                  #
1101  MLCIGLYRFR DTSSSCDASS KRYVITNPPD DFSLLPTDQV FVLMQFDPGL
                      ##
1151  EYKPPAVRAP AGGRGTNTQG SGVGGGGSNK DDNS
                                  #

      Alternative exon A2
 632  ATFRKGVRAVQMVGRAKDDEYSLSN

      Alternative exon B
 745  PPENDANPYAGYQLAYEVKKLM
```

Fig. 4. Deduced amino acid sequence encoded by a composite *slo* cDNA. The hydrophobic domains are underlined. Consensus sites are indicated for cAMP phosphorylation (■) (*35*), PKC-dependent phosphorylation (#) (*35*), a potential ATP-binding site (●) (*31*), and a region containing a potential Ca^{2+}-binding loop (*) (*30*). Below are the deduced amino acid sequences of two alternative exons not included in the composite sequence. Alternative exon A2 is found in cDNA Z8 in the place of exon A1. Alternative exon B is found in cDNAs Z8 and Z54 but missing in CH4. The single letter abbreviations for amino acids are A, Ala; C, Cys; D, Asp; E, Glu; F, Phe; G, Gly; H, His; I, Ile; K, Lys; L, Leu; M, Met; N, Asn; P, Pro; Q, Gln; R, Arg; S, Ser; T, Thr; V, Val; W, Trp; and Y, Tyr. The nucleotide sequence of the composite cDNA has been submitted to GenBank under accession number M69053.

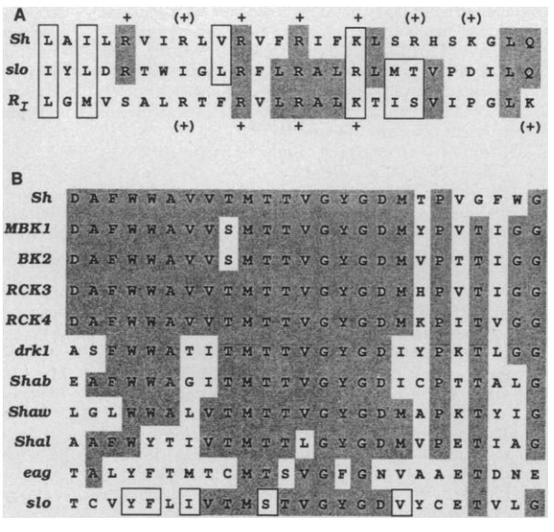

Fig. 5. Alignment of hydrophobic domains S4 and H5 encoded by *slo* with corresponding segments of other channel polypeptides. (**A**) Alignment of S4 domains of *Sh* K^+ channel (top) (*6, 25*), rat brain Na^+ channel type I (R_I) (bottom) (*36*), and *slo* (middle). Amino acid identities are shaded and conservative substitutions are boxed. The positive gating charges in the S4 domain of *Sh* and rat Na^+ channel are indicated. The charges in parentheses are those present in the *Sh* and Na^+ channel sequence but lacking in *slo*. Members of the following groups of amino acids were considered to be conserved: [M, I, L, V]; [A, G]; [S, T]; [Q, N]; [K, R]; [E, D]; [F, Y, W]. (**B**) Alignment of H5 domains of K^+ channels in the *Sh* superfamily (*4, 21*), *eag* (*27*), and *slo*.

determined in *Drosophila*.

Outside these two discrete regions of similarity, the Slo sequence is distinct from all known K^+ channels (*29*). One unusual feature of Slo is its length of 1184 amino acids, including a stretch of about 850 amino acids between the S6 domain and the COOH-terminus, which contains two additional potential membrane-spanning domains. Among other K^+ channels, only Eag (*27*) has a similar length (1174 amino acids). Across the entire hydrophobic core of the polypeptide, Slo shares less than 20% amino acid identity with known K^+ channel sequences. In contrast, members of the extended *Sh* family share at least 35% identity in the core region (*4*). These results define Slo as a distinct type of ion channel polypeptide.

Because the K^+ current affected by *slo* requires intracellular Ca^{2+} for activation, we searched the Slo sequence for an EF hand that would bind Ca^{2+} (*30*). A candidate domain is present near the COOH-terminus (Fig. 4). Although this segment deviates significantly from the consensus EF hand sequence overall, there is very good agreement with the consensus sequence for those residues required for coordinating Ca^{2+} (*30*). A sequence that matches the adenosine triphosphate (ATP)–binding site of tyrosine kinases (*31*) is located in a neighboring region (Fig. 4). Although its effect in *Drosophila* has not been characterized, ATP may directly modulate Ca^{2+}-activated K^+ channels in mammalian smooth muscle (*32*).

Sequence comparisons among *slo* cDNAs indicates that the *slo* transcript is alternatively spliced (Figs. 3 and 4). Alternative splicing of the *Sh* transcript generates a number of gene products with different functional properties (*33*). Whether alternative splicing of *slo* transcripts has similar functional significance is unknown.

The mutant phenotype that results when the *slo* polypeptide is absent or altered allows us to infer the in vivo function of the wild-type gene product. Mutations such as slo^4 cause the selective and complete elimination of I_{CF}, indicating that the *slo* polypeptide is essential for the expression or function of the channels mediating this current. We cloned the *slo* locus solely on the basis of the chromosomal location of these mutations and found that it encodes a polypeptide with sequence similarity to known K^+ channels. Therefore, on the basis of both functional and structural evidence, we propose that Slo is a structural component of Ca^{2+}-activated K^+ channels. Together with *Sh* (*3*) and *eag* (*26, 27*), the *slo* locus defines a third type of K^+ channel structural gene identified and cloned on the basis of its mutant phenotype.

Although the organization of Slo resembles that of other K^+ channel polypeptides, its overall sequence differs extensively from these polypeptides, indicating that the divergence of genes encoding voltage-activated and Ca^{2+}-activated K^+ channels is ancient. The strong conservation of the H5 domain in otherwise divergent channels provides additional support for the fundamental importance of this segment in K^+ channel function. It should now be possible to use *slo* to test emerging models for K^+ selectivity and permeation and to explore the molecular basis for Ca^{2+}-dependent gating.

REFERENCES AND NOTES

1. B. Hille, *Ionic Channels of Excitable Membranes* (Sinauer, Sunderland, MA, 1984).
2. B. Rudy, *Neuroscience* **25**, 729 (1988); R. Latorre, A. Oberhauser, P. Labarca, O. Alvarez, *Annu. Rev. Physiol.* **51**, 385 (1989).
3. A. Kamb, L. E. Iverson, M. A. Tanouye, *Cell* **50**, 405 (1987); D. M. Papazian, T. L. Schwarz, B. L. Temple, Y. N. Jan, L. Y. Jan, *Science* **237**, 749 (1987); O. Pongs *et al.*, *EMBO J.* **7**, 1087 (1988).
4. B. Rudy, C. Kentros, E. Vega-Saenz de Miera, *J. Mol. Cell. Neurosci.* **2**, 89 (1991).
5. L. Salkoff, *Nature* **302**, 249 (1983).
6. T. Elkins, B. Ganetzky, C.-F. Wu, *Proc. Natl. Acad. Sci. U.S.A.* **83**, 8415 (1986).
7. S. Singh and C.-F. Wu, *Neuron* **2**, 1325 (1989); A. Komatsu, S. Singh, P. Rathe, C.-F. Wu, *ibid.* **4**, 313 (1990).
8. B. S. Pallotta, K. L. Magelby, J. N. Barrett, *Nature* **293**, 471 (1981); R. Latorre, C. Vergara, C. Hidalgo, *Proc. Natl. Acad. Sci. U.S.A.* **79**, 805 (1982); C. Miller, E. Moczydlowski, R. Latorre, M. Phillips, *Nature* **313**, 316 (1985).
9. M. Saito and C.-F. Wu, *J. Neurosci.* **11**, 2135 (1991).
10. N. S. Atkinson, G. A. Robertson, B. Ganetzky, *Soc. Neurosci. Abstr.* **15**, 541 (1989); G. A. Robertson, N. S. Atkinson, B. Ganetzky, *ibid.* **16**, 670 (1990); ———, *Biophys. J.* **59**, 196a (1990).
11. D. L. Lindsley and E. H. Grell, *Genetic Variations of Drosophila melanogaster* (Publication No. 627, Carnegie Institution of Washington, Washington, DC, 1968).
12. To isolate new *slo* mutations, wild-type Canton-S males were mutagenized by γ-irradiation (4500 R) and mated to *bar-3* slo^1 females. Among 25,000 F1 male offspring screened, three new mutations exhibiting the *slo* paralytic phenotype (*6*) were recovered. The presence of *bar-3*$^+$ identified the mutagenized chromosome.
13. The electrophysiological phenotype of the new *slo* mutations was assayed by recording action potentials in adult flight muscles in response to stimulation of the motor pathway and direct current injection (*6*) [T. Elkins and B. Ganetzky, *J. Neurosci.* **8**, 428 (1988)]. The defect in I_{CF} was confirmed by voltage-clamp analysis of larval muscles for each new *slo* mutation either when homozygous or in heteroallelic combinations with slo^4.
14. E. Knust, K. Tietze, J. A. Campos-Ortega, *EMBO J.* **6**, 4113 (1987).
15. W. Bender, P. Spierrer, D. S. Hogness, *J. Mol. Biol.* **168**, 17 (1983).
16. The composite cDNA was assembled as follows: nucleotide position 1 to 744 (encoding amino acids 1 to 248) is from cDNA Z54; nucleotide position 745 to 1626 (encoding amino acids 249 to 542) is from cDNA Z8; nucleotide position 1626 to 4232 (encoding amino acids 543 to 1184) is from cDNA CH4. Nucleotide position 1 is the first nucleotide of the open reading frame (ORF) in cDNA Z54. The ORF of Z54 is preceded by a nontranslatable segment lacking a consensus translational start signal. The ORF of CH4 is followed by an untranslated segment of 680 nucleotides terminating in a poly(A)$^+$ tail. DNA was sequenced in M13 and pBluescript (Stratagene) vectors by the dideoxy chain termination method [F. Sanger, S. Nicklen, A. R. Coulson, *Proc. Natl. Acad. Sci. U.S.A.* **74**, 5463 (1977)] with a Sequenase kit (United Biochemical Corp.). All cDNAs were sequenced on both strands. Regions showing GC compression were sequenced with deoxyinosine triphosphate (DITP). Sequence analyses were performed with software from the Genetics Computer Group [J. Devereux, P. Haeberli, O. Smithies, *Nucleic Acids Res.* **12**, 387 (1984)] and the Intelligenetics Molecular Biology Software System (IntelliGenetics, Inc.).
17. cDNAs Z8 and Z54 contain segments judged to be unspliced introns (see Fig. 3A) because of the absence of an ORF, the presence of flanking sequences in agreement with consensus splice sequences [S. Mount, *Nucleic Acids Res.* **10**, 459 (1982)], and sequence comparisons with overlapping cDNAs from which these segments were missing. The untranslated segment at the 5′ end of Z54 preceding the ORF could also be part of an unspliced intron because the first methionine of the open reading frame is not preceded by a consensus translation start site [D. Cavener, *Nucleic Acids Res.* **15**, 1353 (1987)]. Furthermore, unlike Slo, other K^+ channel polypeptides generally have a stretch of 100 to 250 amino acids between the initiating methionine and the first hydrophobic domain (7). If an unspliced intron is present at the 5′ end of Z54, it may include some of the initial sequence present in the conceptual translation (Fig. 4); several potential splice sites occur between the start of the ORF and the S1 domain. A high frequency of unspliced introns in cDNAs encoding a *Drosophila* Na^+ channel has been noted [K. Loughney, R. Kreber, B. Ganetzky, *Cell* **58**, 1143 (1989)].
18. N. J. Proudfoot and G. G. Brownlee, *Nature* **263**, 211 (1976).
19. J. Kyte and R. F. Doolittle, *J. Mol. Biol.* **157**, 105 (1982).
20. W. A. Catterall, *Science* **242**, 50 (1988); W. Stuhmer *et al.*, *Nature* **339**, 597 (1989); D. M. Papazian, L. C. Timpe, Y. N. Jan, L. Y. Jan, *ibid.* **349**, 305 (1991).
21. L. Y. Jan and Y. N. Jan, *ibid.* **345**, 672 (1990).
22. R. MacKinnon, L. Heginbotham, T. Abramson, *Neuron* **5**, 767 (1990), H. A. Hartmann *et al.*, *Science* **251**, 942 (1991).
23. G. Yellen, M. E. Jurman, T. Abramson, R. MacKinnon, *Science* **251**, 939 (1991).
24. A. J. Yool and T. Schwarz, *Nature* **349**, 700 (1991).
25. R. MacKinnon and G. Yellen, *Science* **250**, 276 (1990).
26. R. Drysdale, J. Warmke, R. Kreber, B. Ganetsky, *Genetics* **127**, 497 (1991).
27. J. Warmke, R. Drysdale, B. Ganetzky, *Science* **252**, 1560 (1991); Y. Zhong and C.-F. Wu, *ibid.*, p. 1562.
28. M. Gorczyca and C.-F. Wu, *J. Mem. Biol.* **121**, 237 (1991).
29. One additional region of similarity is the alignment of the S6 hydrophobic domain of Slo with S5 of other K^+ channels. For example, when aligned with the S5 segment of *Sh* there are ten identities and five conservative substitutions among 21 residues. In contrast, the S5 with S5 alignment yields five identities and three conservative substitutions and the S6 with S6 alignment yields four identities and four conservative substitutions. The significance of this alignment between hydrophobic domains that do not occur at corresponding positions is not known.
30. R. M. Tufty and R. Kretsinger, *Science* **187**, 167 (1975); R. H. Kretsinger, *Cold Spring Harb. Symp. Quant. Biol.* **52**, 499 (1987).
31. The consensus sequence for the ATP-binding site in tyrosine kinases is G-X-G-X-X-G-$(X)_{15-20}$-K [M. P. Kamps, S. S. Taylor, B. M. Sefton, *Nature* **310**, 589 (1984)].
32. C. H. Gelband, S. D. Silberberg, K. Groschner, C. van Breemen, *Proc. R. Soc. London Ser. B* **242**, 23 (1990).
33. T. L. Schwarz, B. L. Tempel, D. M. Papazian, Y. N. Jan, L. Y. Jan, *Nature* **331**, 137 (1988); L. C. Timpe, Y. N. Jan, L. Y. Jan, *Neuron* **1**, 659 (1988).
34. Chromosomal in situ hybridization was performed as described [W. Engels, C. Preston, P. Thompson, W. Eggleston, *Focus* **8**, 6 (1986)] except that we used sulfonated (Chemiprobe kit, FMC BioProducts) rather than biotinylated probes.
35. Consensus recognition sequences were (R,K)-

(R,K)-X-S or (R,K)-(R,K)-X-X-S for adenosine 3', 5'-monophosphate (cAMP)-dependent phosphorylation sites [B. E. Kemp, D. J. Graves, E. Benjamini, E. G. Krebs, *J. Biol. Chem.* **252**, 4888 (1977)] and (S,T)-X-(R,K) for protein kinase C (PKC)-dependent phosphorylation [J. R. Woodget, K. L. Gould, T. Hunter, *Eur. J. Biochem.* **161**, 177 (1986); A. Kishimoto *et al.*, *J. Biol. Chem.* **260**, 12492 (1985)].
36. M. Noda *et al.*, *Nature* **320**, 188 (1986).
37. We dedicate this paper to the memory of Tom Elkins, our colleague and friend whose pioneering studies provided the groundwork for this analysis. We thank C. Petersen, and R. Kreber for technical assistance; F. Blattner, L. Marr, and members of the Blattner lab for help with sequencing; E. Knust and J. Campos-Ortega for providing stocks and clones; J. Tamkun, T. Schwarz, L. Jan, Y. N. Jan, B. Hamilton, and E. Meyerowitz for providing libraries; and our colleagues for advice and comments on the manuscript. Supported by NIH grant NS15390, the Markey Charitable Trust, and a Klingenstein Fellowship to B.G. N.S.A. received support from NIH grant T32 GM07131 and the Muscular Dystrophy Association. G.A.R. received support from the American Heart Association of Wisconsin, NIH grant T32 GM07131, and an NIH postdoctoral fellowship. This is paper number 3194 from the Laboratory of Genetics, University of Wisconsin–Madison.

3 May 1991; accepted 18 June 1991

Progressive Encephalopathy and Myopathy in Transgenic Mice Expressing Human Foamy Virus Genes

KATRIN BOTHE, ADRIANO AGUZZI, HANS LASSMANN, AXEL RETHWILM, IVAN HORAK*

Transgenic mice carrying the *bel* region of human foamy retrovirus (HFV) under transcriptional control of its own long terminal repeat expressed the transgene in their central nervous systems and in smooth and striated muscle tissues. The animals developed a progressive degenerative disease of the central nervous system and of the striated muscle. Because expression of the transgene was closely correlated with the appearance of structural damage and inflammatory reactions were scanty, the disease is likely to be caused directly by the HFV proteins. These unexpected findings call for a reevaluation of the pathogenic potential of HFV in humans.

HFV IS A RETROVIRUS ORIGINALLY isolated 20 years ago from individuals with various diseases (*1, 2*). Although the prevalence of HFV was reported to be high in certain geographical areas (*3*), it has not been possible to identify HFV as the causative agent of any human disease (*4*). As with the human T cell lymphoma virus (HTLV) and human immunodeficiency virus (HIV), the HFV genome has, in addition to structural retroviral genes, a region containing three open reading frames, *bel-1* to *bel-3*. Bel-1 has some homology to HIV-2 Tat protein and, similarly to HIV Tat and HTLV-I Tax, functions as a transcriptional transactivator (*5–8*).

Transgenic mice (*9*) have proved useful in the dissection of the pathogenic potential of the regulatory genes of the human retroviruses HTLV-I and HIV (*10*). To analyze the biological activity of HFV regulatory proteins we generated transgenic mice with two constructs: (i) $pHFV_{Af}$, which contains the complete HFV genome in a noninfectious form because of a frameshift mutation in the integrase domain that created a premature stop codon in *pol*, and (ii) pΔgpe, in which 2.3 kb of *gag–pol* and 1.6 kb of *env* were deleted (*7*) (Fig. 1A). In both constructs, expression is controlled by the HFV long terminal repeat (LTR). Eight and nine founder animals (*11*) were derived with $pHFV_{Af}$ and pΔgpe, respectively. Five $pHFV_{Af}$ and six pΔgpe mice developed a neurological syndrome consisting of ataxia, spastic tetraparesis, and blindness. The symptoms in the $pHFV_{Af}$ mice appeared as early as 5 to 6 weeks after birth, progressed rapidly, and led to death within 4 to 6 weeks. The pΔgpe transgenic mice displayed a later onset of the disease (1 to 4 months of age) with a slower progression, which allowed their breeding. The remaining six founder animals, which were asymptomatic, did not express the transgene (*12*). Northern (RNA) hybridization analysis of the expression of the transgene revealed RNAs of sizes corresponding to a total transcript and to *bel* subgenomic mRNA only in the forebrain and in the cerebellum of all animals with disease symptoms (Fig. 1B).

In all animals expressing either construct, the pathological findings were restricted to the central nervous system (CNS) and to the striated muscle. The disease phenotype was transmitted to the offspring with a penetrance of 100%. Animals with the clinical symptoms described above showed variable degrees of selective nerve cell degeneration in the forebrain, with tissue atrophy and reactive gliosis. The areas affected most frequently were the CA3 layer of the hippocampus and the telencephalic cortex (Fig. 2). Some lesions exhibited a more abnormal pattern, with incomplete cortical and subcortical necrosis and occasionally with macrophages and mild lymphocytic infiltrates in the meninges and in the perivascular spaces (*13*). In situ hybridization analysis revealed a complex pattern of expression in the CNS, with groups of neurons, oligodendrocytes, and astrocytes containing high amounts of transcript in the brain and spinal cord. The distribution of positive cells was bilaterally symmetrical. In animals 4 weeks old, most neurons in the CA3 sector of the hippocampus and a subpopulation of cortical neurons were strongly positive for HFV RNA, even in animals in which onset of symptoms had not yet occurred (Fig. 2A). In sick animals older than 6 weeks, most CA3 neurons had degenerated (Fig. 2B), and the highest levels of expression were seen in cortical neurons.

Two $pHFV_{Af}$ and four pΔgpe mice showed focal degeneration of striated mus-

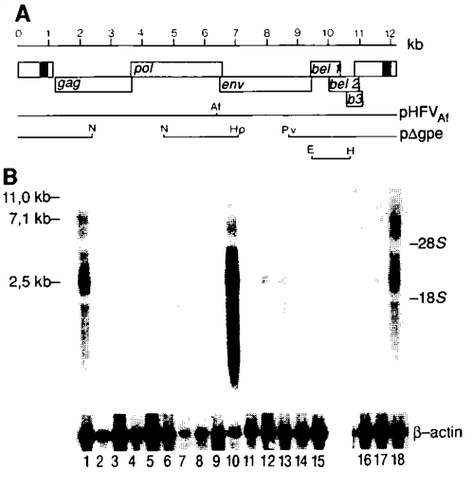

Fig. 1. (**A**) Genomic organization of HFV and constructs used for microinjection. Both constructs have been shown to transactivate HFV transcription in cultured cells (*8*). Af, Afl II; E, Eco RI; H, Hind III; Hp, Hpa II; N, Nco I; Pv, Pvu II. (**B**) Expression of HFV-RNA in various tissues of transgenic mice. Mice 75, 253, 267, and 881 harbor the pΔgpe transgene, and mouse 362 is transgenic for $pHFV_{Af}$. Lanes 1 to 9 were from mouse 75: lane 1, brain; lane 2, liver; lane 3, lung; lane 4, heart; lane 5, thymus; lane 6, kidney; lane 7, muscle; lane 8, lymph nodes; lane 9, spleen. Lane 10, mouse 362 brain; lane 11, mouse 253 testis; lane 12, mouse 253 brain; lane 13, mouse 267 brain; lane 14, nontransgenic littermate brain; lane 15, nontransgenic littermate brain; lane 16, mouse 881 forebrain; lane 17, mouse 881 parietal and midbrain; lane 18, mouse 881 cerebellum and brain stem.

K. Bothe, A. Rethwilm, I. Horak, Institute of Virology and Immunobiology, University of Würzburg, Versbacherstrasse 7, 8700 Würzburg, Federal Republic of Germany.
A. Aguzzi, Research Institute of Molecular Pathology, Dr. Bohr Gasse 7, 1030 Vienna, Austria.
H. Lassmann, Institute of Neurology, Schwarzspanierstrasse 17, 1090 Vienna, Austria.

*To whom correspondence should be addressed.